Journal of ELECTRONIC MATERIALS, Vol. 37, No. 10, 2008
DOI: 10.1007/s11664-008-0514-4

Regular Issue Paper

Air-Gaps for High-Performance On-Chip Interconnect Part I: Improvement in Thermally Decomposable Template

SEONGHO PARK,[1] SUE ANN BIDSTRUP ALLEN,[1] and PAUL A. KOHL[1,2]

1.—School of Chemical and Biomolecular Engineering, Georgia Institute of Technology, 311 Ferst Drive, N.W, Atlanta, GA 30332-0100, USA. 2.—e-mail: paul.kohl@chbe.gatech.edu

The incorporation of air-cavities (i.e., air-gaps) as the intralevel dielectric in integrated circuits (ICs) can provide an ultralow-k solution, especially at the 32 nm technology node and beyond. Air-gaps can be created by the templating method using norbornene (NB)-based sacrificial polymers. However, it has been found that the hardness and modulus of the templating material is critical to achieving mechanical fidelity of the structure during processing. As a result, stiffer sacrificial polymers lead to higher yield. In this study, tetracyclododecene (TD)-based sacrificial polymers were investigated and compared with norbornene-based (NB)-based polymers. Nanoindentation experiments showed that thin films of TD-based sacrificial polymers were harder than NB-based sacrificial polymers. The effect of the modulus and hardness on the process repeatability was quantitatively evaluated by comparing the straightness of 50-nm-wide lines of TD- and NB-based sacrificial polymers. It was shown that the TD-based polymer structures were straighter and had better reproducibility than those of NB-based polymers due to an increase in hardness and modulus. The thermal decomposition properties of TD-based polymers were similar to their NB-based counterparts. Both TD- and NB-based polymers were thermally stable at 300°C and the decomposition residues were less than 1% of the original weight. The thickness of the residue (solid reaction byproducts) from thin TD films was as low as 2.1 nm (depending on the atmosphere quality) and the residue was hydrophobic.

Key words: Air-gap, low-k, Damascene

INTRODUCTION

As the minimum feature size in integrated circuits (ICs) decreases, the number of metal layers increases and their pitch decreases. This increases the resistance–capacitance (RC) time constant, cross talk, and energy dissipation. Thus, the International Technology Roadmap for Semiconductors (ITRS) calls for a decrease in capacitance by lowering the dielectric constant (k) of the metal insulator.[1] Among the low-k options, the incorporation of air, in the form of air-gaps, is the lowest dielectric constant available. Air-gaps are most valuable when integrated as the intrametal dielectric (IMD) material of local interconnects. Air-gaps have been fabricated by selective plasma deposition where a cavity is intentionally produced during deposition[2] or by removing one of the materials in the build-up process once the metal–insulator stack has been fabricated. The selective removal of a placeholder material can be achieved by thermal decomposition of a sacrificial polymer[3,4] or by wet etching.[5] In this study, an improvement in the thermally decomposable sacrificial polymer, used as a placeholder to fabricate air-gaps in the IMD layer, is described.

The fabrication process flow for the integration of air-gaps using a thermally decomposable polymer as a place holder is shown in Fig. 1. The sacrificial polymer is spin-coated on the substrate followed by the deposition of SiO_2, which serves as the hard mask and chemical mechanical polishing (CMP)

(Received December 23, 2007; accepted June 10, 2008; published online July 29, 2008)

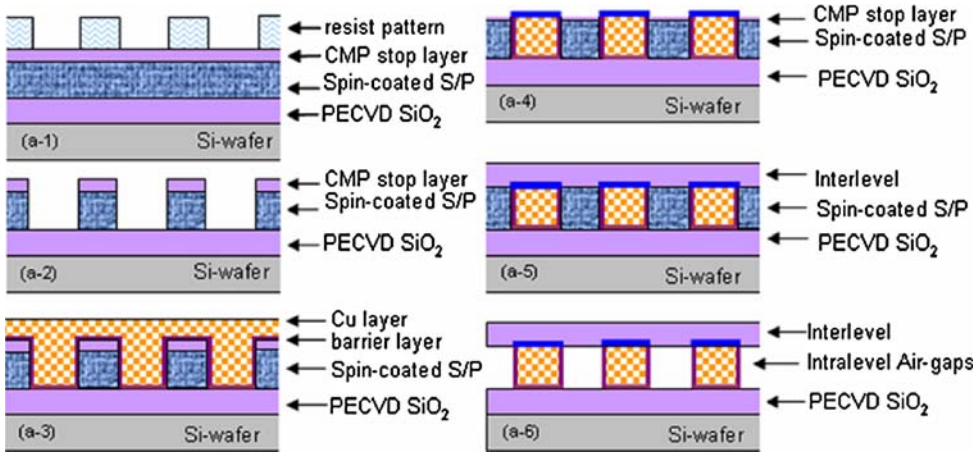

Fig. 1. Schematic diagram of the fabrication process of the single-layer Cu/air-gap interconnect structure.

stop-layer. Photoresist is used to transfer the pattern to the SiO_2 and the sacrificial polymer is dry-etched. The next steps include the deposition of a metal barrier and Cu seed layer, and the electroplating of Cu. The excess Cu is removed by CMP, and the capping layer is deposited on top of Cu lines. After deposition of the encapsulating material (interlayer dielectric), the sacrificial polymer between Cu lines is removed by thermal decomposition, resulting in the formation of cavities (i.e., air-gaps). The gaseous byproducts in the cavities between metal conductors permeates through the overcoat material at the polymer decomposition temperature, and the pressure in the cavity quickly comes into equilibrium with the ambient atmosphere. High-aspect-ratio structures (height-to-width) of the interconnects are desired to improve the electrical performance. The mechanical integrity of the free-standing sacrificial polymer structures is critical to the reproducibility of the process over large areas. In addition, the sacrificial polymer must be thermally stable during plasma-enhanced chemical vapor deposition (PECVD) of the overcoat material. Residue left from the thermal decomposition of the sacrificial polymer should be minimized as it increases the effective dielectric constant of the air-gap. It is also important that the air-gap surface is hydrophobic, so that moisture is not absorbed in the cavity. The presence of moisture increases the dielectric constant and may facilitate corrosion of the metal.

Therefore, the thermal, mechanical, and chemical properties of the sacrificial polymer and its products are critical to the performance and reliability of final copper/air-gaps interconnect structures. In this study, the mechanical integrity of the free-standing sacrificial polymer structures was studied. The ability to form and maintain straight polymer lines during subsequent processing (e.g., metallization and CMP) is critical to the yield and electrical properties of the final interconnect structures. Any deformation or distortion of the sacrificial polymer will results in distortion in the metal lines. The polymer structures can elastically or plastically deform and temporary and permanent stresses are applied to the polymer during processing. It is highly desirable to have the sacrificial polymers which do not deform, by elastic, plastic or creep mechanisms.

Norbornene-based (NB) thermally decomposable polymers (Unity4011^{TM}, Promerus LLC.) have been used as sacrificial placeholders to fabricate air-gaps in IMD layers.[3,6] However, in the fabrication of dual Damascene air-gaps using sacrificial polymers, high-aspect-ratio lines and anisotropic etching of the sacrificial polymer are required. The sacrificial polymer must withstand CMP processes as well. Thus, sacrificial polymers which resist deformation, whether by elastic or plastic mechanisms, are of interest for improved process yield. In a previous study,[7] thin films of an NB sacrificial polymer were exposed to an electron beam in order to make them harder and have a higher modulus. However, irradiation of the sacrificial polymer by an electron beam resulted in degradation of the thermal properties of the polymer. In this study, a tetracyclododecene (TD)-based sacrificial polymer (Unity4131^{TM}, Promerus LLC), which has a more rigid molecular structure compared with the NB-based sacrificial polymer (Fig. 2), was investigated for use as a sacrificial polymer in the formation of air-gaps.

NB- and TD-based polymers are both cyclic olefins. It is known that cyclic olefin copolymers have a high glass-transition temperature, optical clarity, low shrinkage, low moisture absorption, and low birefringence.[8–10] Due to the more rigid molecular structure of the TD-based versus the NB-based polymer, it is expected that the TD-based sacrificial polymer will be harder and will lead to improved process repeatability. In this study, the thermal and mechanical properties of a TD-based sacrificial polymer were compared with those of an NB-based

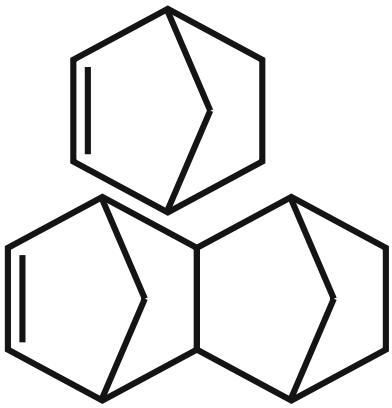

Fig. 2. The chemical structures of monomer units of (a) norbornene (NB) and (b) tetracyclododecene (TD) sacrificial polymers.

sacrificial polymer using dynamic thermal gravimetric analysis (TGA) and nanoindentation. In addition, in order to investigate the effect of the modulus and hardness of the polymers on the process reliability, 50 nm lines of both polymers were fabricated using electron beam lithography and reactive ion etching (RIE). The straightness of the lines as well as the chemical properties of the residue were evaluated.

EXPERIMENTAL

Both TD- and NB-based sacrificial polymers were provided by Promerus LLC (Brecksville, OH). For the thin-film samples, the polymers were spin-coated on Si wafers and soft-baked at 110°C for 5 min on a hot plate. After soft-baking, the polymer films were hard-baked at 300°C for 1 h in a furnace to remove residual solvent and volatile components. For the analysis of thermal decomposition residues of sacrificial polymers, hard-baked thin films were thermally decomposed in a furnace at 450°C for 2 h with a ramp rate of 2°C/min. Before increasing the temperature, nitrogen gas was used to purge the furnace (4 L/min) for 30 min to remove residual oxygen. During heating, the nitrogen gas flow rate was 2 L/min. Experiments were performed to determine the effect of purging gas (nitrogen purity) on the amount of decomposition residues. Three different purging gas conditions were considered: (A) 2 L/min N_2, normal purging condition, (B) a mixture of 1.5 L/min N_2 and 0.5 L/min H_2, adding hydrogen, and (C) 4 L/min N_2 (double the normal nitrogen flow rate). Oxygen concentrations for each purging condition were measured using a Series 3000 Trace Oxygen Analyzer (ALPHA OMEGA Instrument Corp., Cumberland, RI, USA).

The stress–strain behavior of thin-film sacrificial polymers was measured by using a TriboIndenter nanoindenter (Hysitron Inc. Minneapolis, MN). The indentation system was enclosed in an acoustic housing and located on an antivibration table. For indentation, the *Z*-axis resolution was 0.04 nm and a three-sided Berkovich tip was used. The radius of

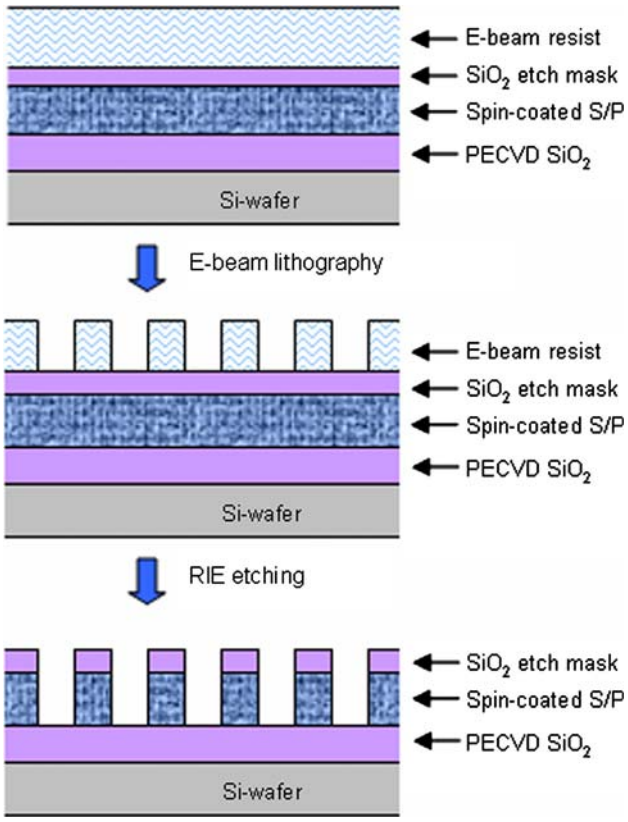

Fig. 3. The fabrication processes of sacrificial polymer lines, 50 nm in width and 85 nm in height.

curvature of the Berkovich tip was between 100 nm and 200 nm. To exclude the effect of the substrate, the maximum force was chosen so as to indent less than 10% of the film thickness.[11]

The effect of the modulus and hardness of the sacrificial polymers on process repeatability was evaluated by scanning electron microscopy (SEM) imaging of the 50 nm polymer lines. In the 2006 version of the ITRS,[1] the metal 1 wiring pitch is 104 nm in 2009 and 90 nm in 2010. In addition, the aspect ratio of metal 1 wiring is 1.8 in both 2009 and 2010. In order to match these design rules, sacrificial polymer lines and spaces of 50 nm, and 1.7:1 (*H*:*W*) aspect ratios were fabricated. The fabrication schematic for the 50 nm polymer lines is shown in Fig. 3. SiO_2 (5 μm thickness) was deposited using PECVD and the sacrificial polymers were spin-coated. The films were soft-baked at 110°C for 5 min and hard-baked at 300°C for 1 h in a furnace. After hard-baking, the final polymer thickness was 85 nm. Thirty nanometers of PECVD SiO_2 was deposited as a hard mask on top of the hard-baked polymer films. Polymethylmethacrylate (PMMA) positive tone electron-beam resist was spin-coated on the SiO_2 hard mask; the thickness of PMMA was 80 nm. PMMA patterns (50 nm width and 4 mm length) were fabricated using a JEOL JBX-9300FS electron-beam lithography system. The accelerating voltage of the electron beam was 100 kV and the minimum spot size was 4 nm. The beam

current was 2 nA and the electronic dose was 450 $\mu C/cm^2$. The developing time for PMMA patterns was 35 s using a 1:1 volume ratio of methyl isobutyl ketone and isopropyl alcohol. After developing, the PMMA patterns were transferred to the SiO_2 hard mask and the sacrificial polymer layer by reactive ion etching (RIE). In order to etch the SiO_2 hard mask, an RIE gas mixture of 45 sccm CHF_3 and 5 sccm O_2, at 200 W radiofrequency (RF) power was used. The RIE conditions for the polymers were 45 sccm O_2, 0.5 sccm CHF_3, and either 300 W or 400 W RF power. After fabricating the sacrificial polymer lines, 25 top-view SEM images were taken for both the TD- and NB-based polymers. The SEM magnification was fixed at 20 k and the total length of the sacrificial polymer lines was 3981.25 μm. To quantify the linearity of the sacrificial polymer lines, SEM pictures were transformed into binary images. In a binary image, the number of pixels was 650×1024 (row $\times$ column), and the pixel position and width of the polymer line at each row was determined using the difference in contrast between the polymer lines and the space. The center line position of each polymer line was calculated using the information about the pixel position. The center line was determined by connecting the center of the first row and the last row (the 650th row) in a polymer line. The deviation from a straight line was calculated .

The properties of the sacrificial polymers were investigated using dynamic TGA using a Seiko Instruments Inc. 320 thermogravimetric differential thermal analyzer (Haake Instrument, Paramus, NJ). The sacrificial polymer films were removed from the wafer surface and placed in a TGA sample pan. In the TGA experiment, nitrogen gas was purged for 30 min before the run. The heating rate was 2°C/min from room temperature to 550°C.

The thickness and composition of decomposition residues of the polymers were investigated using x-ray photoelectron spectroscopy (XPS) and depth profiling. XPS measurements were carried out with a Physical Electronics model 1600 XPS system using an aluminum $K\alpha$ source and toroidal monochromator. The spot size was 0.8 mm and take-off angle was 45 deg. The base pressure was less than 5×10^{-9} Torr. Ar-ion sputtering was used for depth profiling. The thickness of the films was estimated and compared to each other. The Ar-ion sputtering rate was calibrated by depth profiling of a known thickness of sacrificial polymer layer; the calibrated etch rate was 2.9 nm/min. It was assumed that the sputter etch rate for a polymer layer was the same for the decomposition residue. For the XPS experiment, a 250 nm Al layer was deposited on the Si wafer using DC sputtering and then the polymers were spin-coated. Spin-coated polymer thin films were soft-baked at 110°C for 5 min on the hot plate and then hard-baked at 300°C for 1 h in a furnace to remove the residual solvent and volatile elements. For reference purposes, a bare aluminum layer on a Si wafer without the sacrificial polymer layer was heat-treated and depth-profiled to serve as the end-point detection.

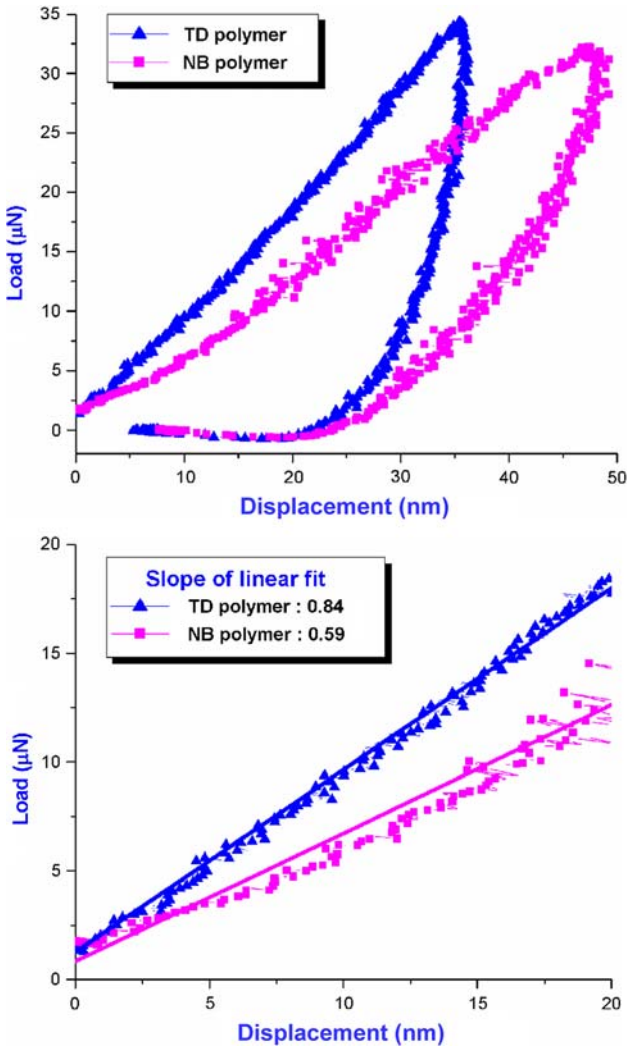

Fig. 4. The load–displacement curves of thin films of TD- and NB-based sacrificial polymers using a nanoindenter.

The elemental mapping images of the decomposition residues were taken using time-of-flight secondary-ion mass spectroscopy (TOF-SIMS, CAMECA ION-TOF IV) with a mapping area of 70 μm $\times$ 70 μm. A gallium ion gun with the ion energy of 1.5 keV was used.

The hydrophobicity of the sacrificial polymer thin films and decomposition residues was evaluated by measuring the contact angle of a water drop on the surface of the samples using a VGA 2500XE (Video Contact Angle System, AST Product Inc., Billerica, MA). The measurements were repeated ten times for each sample and the contact angles were averaged.

RESULTS AND DISCUSSION

The load–deflection behavior of the TD- and NB-based polymers was measured using nanoindentation and is shown in Fig. 4. The maximum

load was chosen in order to indent less than 10% of the thickness of thin films so that substrate effects were excluded.[11] Figure 4a shows the full range of the indentation and Fig. 4b shows the initial part of the indentation force–deflection curve. The NB-based polymer was evaluated at the same load. The greater indentation depth for the NB-based polymer is due to its lower modulus and hardness. For example, at a load of 20 μN, the indentation depth of the TD- and NB-based polymers were 21.6 nm and 29.5 nm, respectively. The initial part of the load–deflection curve was used to compare the properties qualitatively. In Fig. 4b, the slopes of the initial portion of the indentation curves were 0.84 μN/nm and 0.59 μN/nm for the TD- and NB-based polymer, respectively. The smaller indentation depth and larger slope for the TD-based polymer shows that the TD-based polymer is more resistant to deformation than the NB-based sacrificial polymer. This stiffness has both an elastic and plastic component, which was not further quantified because any deformation, regardless of the mechanism, is undesirable. For quantification, the procedure developed by Oliver and Pharr[12] was used to calculate the hardness. In this quantification, the slope of the load deflection curve at low loads will be used and Pharr's terminology will be adopted. No additional analysis between elastic and plastic effects will be considered. The contact stiffness was calculated by fitting the unloading data between 20% and 95% to the power-law relationship in Eq. 1 along with Eq. 2.

$$P = \alpha(h - h_f)^m, \tag{1}$$

$$S = \frac{dP}{dh}, \tag{2}$$

where P is the indentation load (μN), h is the indenter displacement (nm), h_f is the final indentation depth (nm), α and m are fitting parameters, and S is the contact stiffness (μN/nm). The contact stiffness was used to calculate the hardness (H) by means of Eqs. 3 and 4.

$$h_c = h_{max} - 0.75\frac{p_{max}}{S}, \tag{3}$$

$$H = \frac{P_{max}}{A(h_c)}, \tag{4}$$

where h_c is the contact depth (nm), h_{max} is the maximum indentation depth (nm), P_{max} is the maximum load (μN), and $A(h_c)$ is the indentation contact area (nm^2), which is a function of depth. For a pyramidal geometry tip (Berkovich), the relationship between the indentation contact area and the contact depth is given by Eq. 5.

$$A(h_c) = 24.5h_c^2 \tag{5}$$

The calculated hardness (H), contact stiffness (S), and the maximum indentation depth are summarized in Table I. The calculated hardness of the thin films of TD- and NB-based polymers were 1.3 GPa and 0.8 GPa, respectively.

The effect of hardness on the process repeatability of TD- and NB-based sacrificial polymers was investigated by fabricating 50 nm polymer lines and carrying out image processing for evaluation of line straightness. Figure 5 shows a top view of the sacrificial polymer lines, the calculated center line, and the ideal straight center line. The absolute value of the deviation from a straight line will be presented. In this way, the straightness of the TD- and NB-based polymer lines can be seen.

The SiO_2 hard mask patterns formed by RIE on top of the TD- and NB-based polymers are shown in Fig. 6. Two different RIE power levels (300 W and 400 W) were used to transfer the SiO_2 patterns to the TD- and NB-based polymers, as shown in Fig. 7. Two different magnifications of SEM images for each polymer are shown in Fig. 7 in order to show the difference of the line shapes between the two polymers. On the right-hand side of Fig. 7, a higher magnification SEM image shows that the NB-based polymer lines were not as straight as the TD-based polymer lines. In the dual Damascene processes, straight-walled polymers are critical. Deformation of the polymer would result in distortion of the metal line.

In order to quantify the straightness of each polymer, 25 plan-view SEM images were taken and processed for each polymer. The average distortion of the lines and standard deviation are summarized in Table II. At 300 W RF power, the average distortion of 50 nm TD and NB lines was 1.6 nm and 4.0 nm, respectively. At 400 W RF power, the distortion was 1.6 nm and 3.4 nm for TD and NB lines, respectively. It can be seen that the harder TD-based sacrificial polymer has better process reproducibility than the softer NB-based polymer.

Dynamic TGA analysis for the TD- and NB-based polymers is shown in Fig. 8. The TGA data for the TD-based polymer is essentially the same as that for

Table I. Nanoindentation Results for Thin Films of TD- and NB-Based Sacrificial Polymers

	TD-Based Polymer	NB-Based Polymer
Hardness (GPa)	1.3	0.8
Contact stiffness (μN/nm)	6.5	2.5
Maximum indentation depth (nm)	35.7	49.2

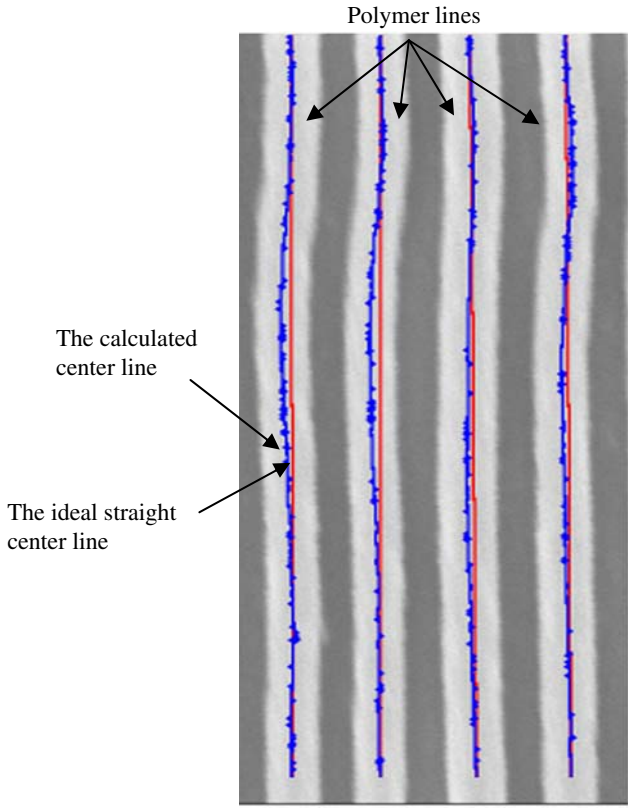

Fig. 5. Sample image to determine the ideal straight center lines and the calculated center lines reflecting the actual shapes of polymer lines, NB-based sacrificial polymer, RF power = 300 W. Each line and space is 50 nm.

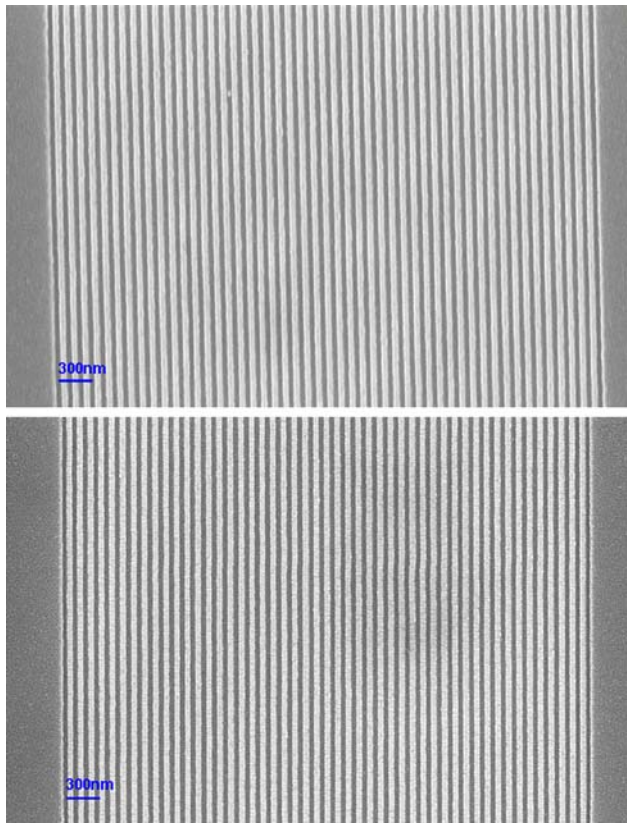

Fig. 6. Top view scanning electron microscopic images of the patterns of SiO_2 hard mask on top of hard-baked sacrificial polymer layers.

the NB-based polymer. Both TD- and NB-based polymers were thermally stable up to 300°C (e.g., the temperatures for 5% weight loss were 353°C for the TD-based polymer and 357°C for the NB-based polymer). The temperature range for weight loss between 5% and 95% loss was from 353°C to 445°C for TD and from 357°C to 441°C for NB. The decomposition residue at 550°C for TD and NB was 0.33% and 0.70%, respectively. From the dynamic TGA analysis, it was concluded that TD-based material has similar thermal properties to NB.

The dynamic TGA analysis shows that the amount of residue after decomposition was insignificant. XPS depth profiling using an Ar-ion gun was used to evaluate the thickness and composition of the decomposition products. The XPS depth profiling to the decomposition residues was performed after decomposition of a 300-nm-thick film of TD-based polymer when the chamber was purged to different purity levels. The results are summarized in Fig. 9.

Figure 9a shows the depth profile for an Al layer on a silicon wafer which experienced the same heating profile as when the polymer was present. In the depth profiles, the crossover between the carbon and aluminum signals was taken as the interface between the residue and substrate onto which the polymer was deposited. In the case of bare Al, the carbon layer was formed by atmospheric carbon and the crossover occurred at 0.7 min etching time. In the case of the TD-based polymer residue with purging conditions A, B, and C (see the "Experimental Section" for details), the crossover points were 5 min, 0.75 min, and 1 min, respectively. The thickness of the residues was similar to atmospheric carbon except in the case of purging condition A. According to previous studies,[8,11] a higher oxygen content results in more residue. The measured oxygen content with purging condition A was 55 ppm and it decreased to 19.6 ppm when hydrogen was added to the purging gas (condition B). In addition, the estimated oxygen concentration under purging condition C was 21.7 ppm. Hydrogen acts as a reducing agent and decreases the oxygen concentration in the furnace, resulting in less residue. In addition, an increase of nitrogen flow rate from purging condition A to condition C decreases the oxygen concentration in the furnace and lowers the amount of residue.

The ion sputter etch rate of the polymer was 2.9 nm/min. The sputter etch rate of an element is determined by its sputtering yield, which is the average number of atoms removed in any state per incident particle.[13,14] Furthermore, the sputtering

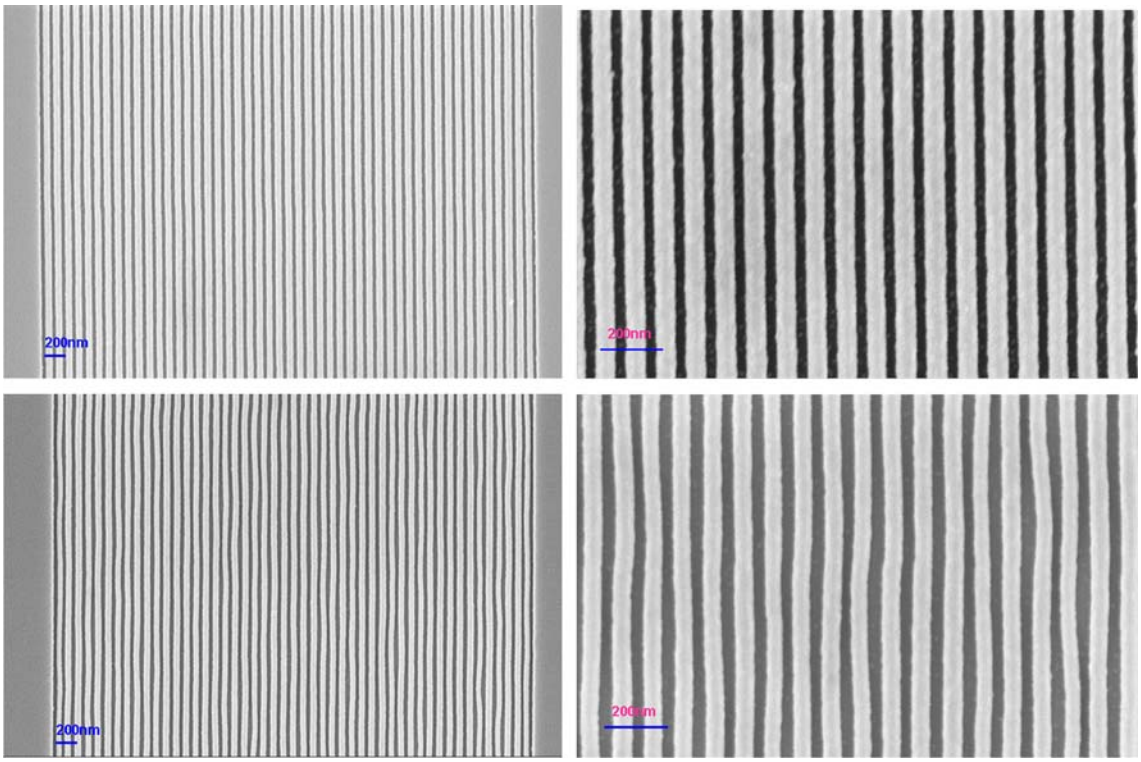

Fig. 7. Top view scanning electron microscopic images of the lines of TD- and NB-based sacrificial polymers, RF power = 400 W.

Table II. Summary of SEM Image Processing for the Evaluation of the Linearity of TD- and NB-Based Sacrificial Polymer Lines

	NB Polymer, RF = 300 W	TD Polymer, RF = 300 W	NB Polymer, RF = 400 W	TD Polymer, RF = 400 W
Average distortion per pixel (5 nm × 5 nm)	4.0 nm	1.6 nm	3.4 nm	1.6 nm
Standard deviation	3.9 nm	2.4 nm	3.5 nm	2.4 nm

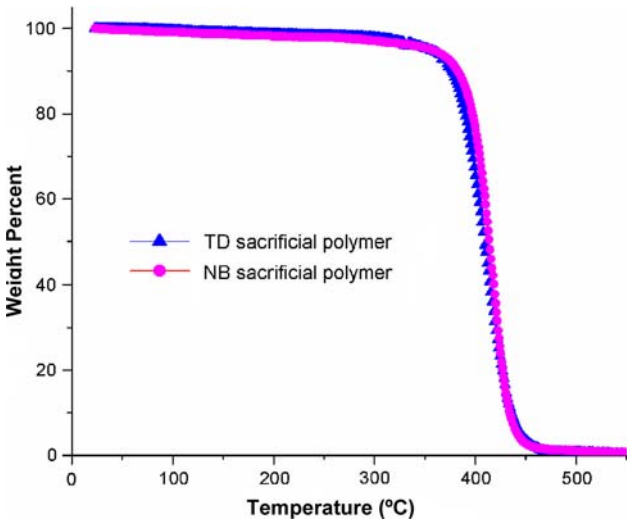

Fig. 8. Dynamic TGA of TD- and NB-based sacrificial polymers.

yield depends on the energy and the mass of the incoming projectiles and target atoms, and the angle of incidence of the projectiles. With the given energy and angle of the incident Ar-ion beam, the sputtering yield depends on the mass ratio of the target atoms to the incident ion beam. The polymers and their residues are composed of mostly carbon and oxygen. The mass ratios of carbon and oxygen to the incident projectile (argon) are 0.3 and 0.4, respectively, and are close to each other compared with that of aluminum or silicon, indicating that the sputtering yield and etch rate of carbon are similar to those of oxygen. Therefore, it was assumed that the sputter etch rate of the residues and contaminated layer are the same as that of the polymers. The crossover at 0.7 min etching time of bare Al in the depth profile indicates that the estimated thickness of carbon layer contaminated from the atmosphere was 2.0 nm.

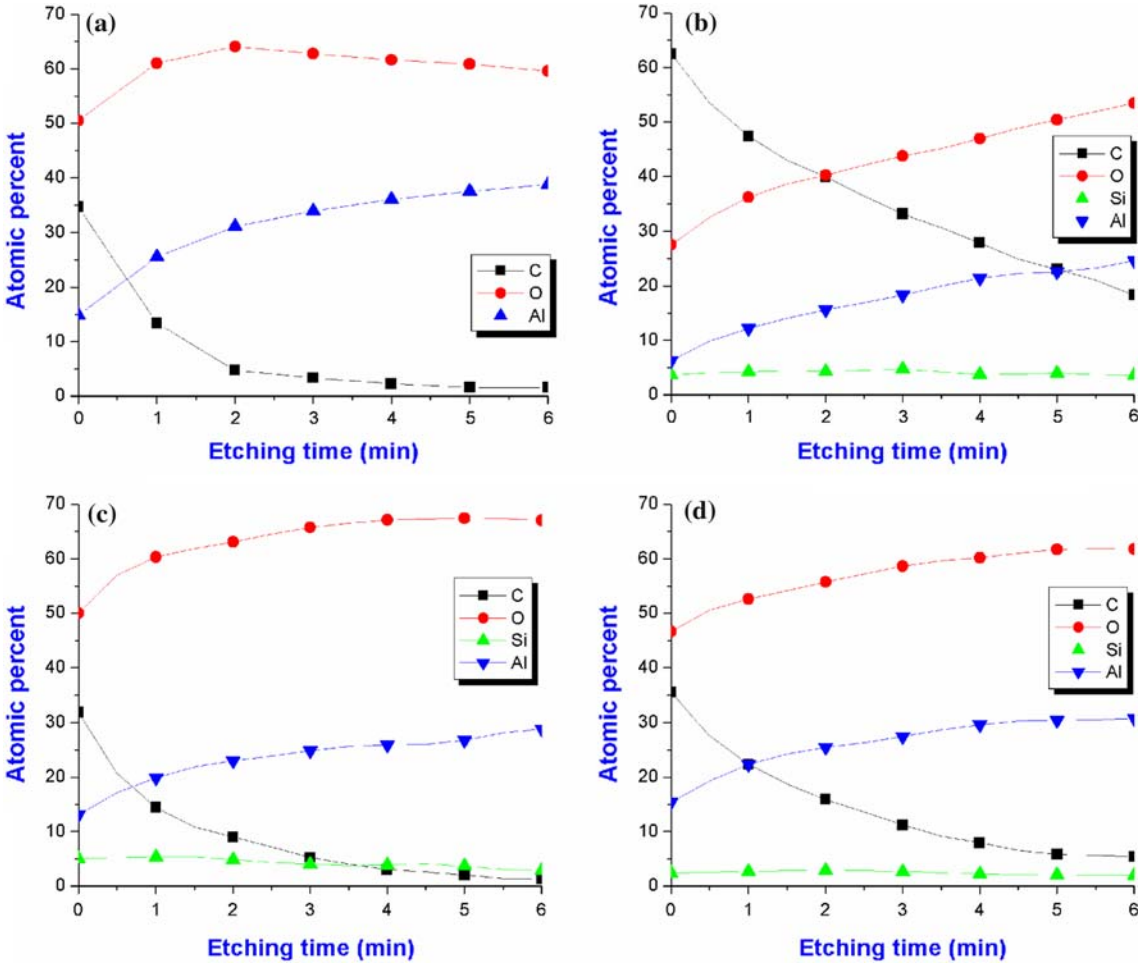

Fig. 9. XPS depth profiling of the decomposition residues of a TD-based sacrificial polymer with different purging conditions during the thermal decomposition: (a) bare Al on Si-wafer, (b) purging condition A, (c) purging condition B, and (d) purging condition C.

Based on an etch rate of 2.9 nm/min using known polymer thicknesses as a calibration standard, the estimated thickness of the residues was 14.5 nm for purging condition A, 2.1 nm for purging condition B, and 2.9 nm for purging condition C. In the case of purging condition A, even though the estimated thickness of residue was 14.5 nm, Al was detected at the zero etching time (Fig. 9b). This indicates that the residue was not a homogeneous layer. This was confirmed by SIMS elemental maps of the decomposition residues, as shown in Fig. 10. The carbon and silicon elemental maps show the distribution of elements in the polymer residues. The silicon resulted from a silyl-ether side group in the polymer, used for adhesion.

The atomic compositions of the TD films and decomposition residues are summarized in Table III along with the atomic composition after 3 min Ar-ion sputter etching. The TD polymer was hard-baked at 300°C for 1 h. In the case of bare Al, the carbon resulted from atmospheric contamination. The residual oxygen and silicon were from the silyl-ether adhesion promoter in the polymer. After 3 min of Ar-ion sputter etching, the carbon content of the residue was 5.3 at.% and 11.2 at.% for purging conditions B and C, respectively. They were comparable to the carbon content of bare Al (3.4 at.%) after 3 min of Ar-ion sputter etching, indicating a thin residue layer. However, the carbon content in the case of purging condition A was 33.2 at.%, indicating a thicker residue layer.

The hydrophobicity of the residue surface after decomposition is critical because moisture would increase the dielectric constant and could lead to corrosion of the copper. The hydrophobicity was investigated by measuring the contact angle of a water drop. The polymer samples were hard-baked at 300°C for 1 h and thermally decomposed under different purging conditions. The contact angles for the polymer residues was larger than those of the

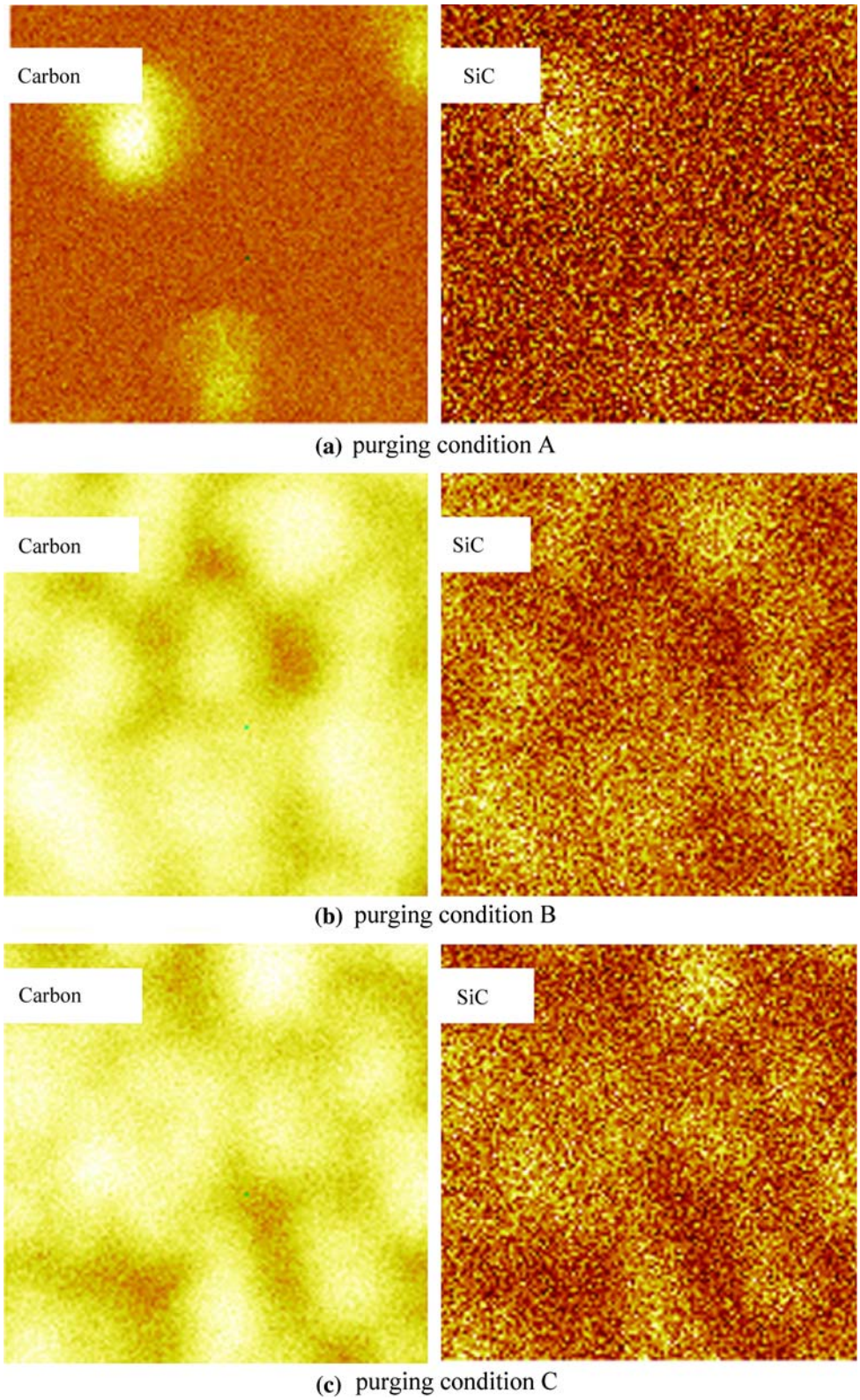

Fig. 10. TOF-SIMS carbon and SiC elemental mapping images of decomposition residues of TD-based sacrificial polymer: (a) purging condition A, (b) purging condition B, and (c) purging condition C. Each image is a 1 μm field.

aluminum films, as shown in Table IV. Two polymer thicknesses were used in the experiments in order to investigate the effect of the initial thickness on the hydrophobicity of the surface after decomposition. As shown in Table IV, there was no clear difference in contact angle between the thin and thick

Table III. Atomic Composition of Thin Films and Decomposition Residues of TD-Based Sacrificial Polymer

Percent Composition		Carbon	Oxygen	Silicon	Aluminum
Bare Al	As-received	34.7	50.5		14.8
	After 3 min etching	3.4	62.8		33.9
Hard-baked thin films of TD polymer	As-received	95.5	3.9	0.7	
	After 3 min etching	94.6	4.9	0.5	
Decomposed TD, purging condition A	As-received	62.5	27.5	3.7	6.3
	After 3 min etching	33.2	43.8	4.8	18.3
Decomposed TD, purging condition B	As-received	31.8	50.0	5.1	13.1
	After 3 min etching	5.3	65.8	4.1	24.9
Decomposed TD, purging condition C	As-received	35.5	46.7	2.4	15.4
	After 3 min etching	11.2	58.7	2.7	27.4

Table IV. Summary of the Contact-Angle Measurements of the Polymer Films Itself and Decomposition Residues of TD- and NB-Based Sacrificial Polymers with Variation of the Purging Gases and the Initial Thickness of the Polymer Thin Films

(Degrees)	Hard-Baked Thin Films	Decomposed, Purging Condition A	Decomposed, Purging Condition B	Decomposed, Purging Condition C
Bare Al	71.6	39.2	54.2	46.0
TD polymer (300 nm)	95.7	91.9	87.5	85.2
TD polymer (1.2 μm)	95.1	85.0	87.8	86.9
NB polymer (400 nm)	100.8	83.8	84.4	
NB polymer (4.5 μm)	98.5	99.8	89.3	

polymer films for either TD- and NB-based polymers. In addition, the different purging gas conditions had no effect on the hydrophobicity of the residue surfaces. The large carbon content in the residue resulted in a hydrophobic surface with a large contact angle.

CONCLUSIONS

Nanoindentation experiments have shown that the TD-based polymer was more resistant to mechanical deformations compared with an NB-based polymer. The effect of hardness on the process repeatability was investigated by fabricating 50 nm polymer lines and performing image processing for the evaluation of straightness. It was shown that the harder TD polymer had better process repeatability than the softer NB polymer. From the dynamic TGA analysis, the TD-based polymer had similar thermal properties to the NB-based polymer. Both TD- and NB-based polymers were thermally stable up to 300°C, and the decomposition residues were less than 1% of the initial polymer thickness. The surfaces of the polymer films and their residues were hydrophobic.

ACKNOWLEDGEMENT

The authors gratefully acknowledge the support of Promerus LLC.

REFERENCES

1. The International Technology Roadmap for Semiconductors (2007). http://www.itrs.net/.
2. T. Harada, A. Ueki, K. Tomita, K. Hashimoto, J. Shibata, H. Okamura, K. Yoshikawa, T. Iseki, M. Higashi, S. Maejima, K. Nomura, K. Goto, T. Shono, S. Muranka, N. Torazawa, S. Hirao, M. Matsumoto, T. Sasaki, S. Matsumoto, O. Ogawa, M. Fujisawa, A. Ishii, M. Matsuura, and T. Ueda, *IEEE International Interconnect Technology Conference* (San Francisco, CA, 2007), p. 141.
3. P. Kohl, D. Bhusari, M. Wedlake, C. Case, F. Klemens, J. Miner, B. Lee, R. Gutmann, and R. Shick, *Electron. Dev. Lett.* 21, 557 (2000).
4. R. Daamen, P.H.L. Bancken, D. Ernur Badaroglu, J. Michelon, V.H. Nguyen, G.J.A.M. Verheijden, A. Humbert, J. Waterloos, A. Yang, J.K. Cheng, L. Chen, T. Martens, and R.J.O.M. Hoofman, *IITC* (San Francisco, CA, 2007), p. 61.
5. L.G. Gosset, F. Gaillard, D. Bouchu, R. Gras, J. de Pontcharra, S. Orain, O. Cueto, Ph. Lyan, O. Louveau, G. Passemard, and J. Torres, *IITC* (San Francisco, CA, 2007), p. 58.
6. S.H. Park, J. Krotine, S.A. Bidstrup, and P.A. Kohl, *208th ECS Conference* (Los Angeles, CA, 2005).
7. S. Park, J. Krotine, S. Bidstrup Allen, and P. Kohl, *J. Electron. Mater.* 35, 1112 (2006).
8. G. Khanarian and H. Celanese, *Opt. Eng.* 40, 1024 (2001).
9. D. McNally, *Plast. Eng.* 56, 51 (2000).
10. N. Grove, *Characterization of Functionalized Polynorbornenes as Interlevel Dielectrics* (Ph.D dissertation, Georgia Institute of Technology, 1997).
11. T.Y. Tsui and G.M. Pharr, *J. Mater. Res.* 14, 292 (1999).
12. W.C. Oliver and G.M. Pharr, *J. Mater. Res.* 7, 1564 (1992).
13. A. Czanderna, T. Madey, and C. Powell, *Methods of Surface Characterization—Volume 5: Beam Effects, Surface Topography, and Depth Profiling in Surface Analysis* (Kluwer Academic Publishers: Norwell, MA, 2002).
14. P. Sigmund, *Phys. Rev.* 184, 383 (1969).